



## Research papers

# Space-time evolution of land subsidence in the National Capital Region of India using ALOS-1 and Sentinel-1 SAR data: Evidence for groundwater overexploitation



Hrishikesh Kumar<sup>a,d</sup>, Tajdarul Hassan Syed<sup>b,\*</sup>, Falk Amelung<sup>c</sup>, Ritesh Agrawal<sup>a</sup>, A. S. Venkatesh<sup>d</sup>

<sup>a</sup> Space Applications Centre, Indian Space Research Organization, Ahmedabad, India

<sup>b</sup> Department of Earth Sciences, Indian Institute of Technology Kanpur, India

<sup>c</sup> Department of Marine Geosciences-Rosenstiel School of Marine and Atmospheric Science, University of Miami, USA

<sup>d</sup> Department of Applied Geology, Indian Institute of Technology (ISM) Dhanbad, India

## ARTICLE INFO

This manuscript was handled by Jiri Simunek, Editor-in-Chief, with the assistance of Todd C. Rasmussen, Associate Editor

## ABSTRACT

Land subsidence due to groundwater extraction is increasingly becoming a major scientific and societal issue. In this study, ALOS-1 (2007–10) and Sentinel-1 (Nov. 2014–19) datasets are utilized to compute vertical land subsidence in the National Capital Region (NCR) of India. Two major subsidence zones located in Dwarka ( $12 \text{ km}^2$ ) and Gurgaon ( $1 \text{ km}^2$ ) area, showing subsidence rate up to  $6.0 \text{ cm/year}$ , are observed during 2007–10. Between Nov. 2014–19, while a substantial reduction in the size (by  $\sim 6 \text{ km}^2$ ) and subsidence rate (by  $\sim 3 \text{ cm/year}$ ) is observed for the zone in Dwarka, significant enlargement (by  $\sim 11 \text{ km}^2$ ) and enhanced subsidence rate (by  $5 \text{ cm/year}$ ) are observed for the zone in Gurgaon. An emerging subsidence zone ( $4.5 \text{ km}^2$ ) subsiding at  $3.6 \text{ cm/year}$  is also detected in the Faridabad area. The deceleration of subsidence in the Dwarka area is due to stabilization of groundwater level post-2014. Residual compaction of the aquifer system in the Dwarka area halted after Sept. 2016, and at present, it shows elastic deformation. In Gurgaon and Faridabad, dominantly negative linear trends in vertical displacement, lack of seasonal signals, and ongoing groundwater depletion indicate continuous inelastic deformation of the aquifer system. The preferential disposition of subsidence zones on the western part of Delhi ridge indicates a dominantly confined aquifer system and aquifer compartmentalization by the Delhi ridge. Results presented here demonstrate that precise subsidence monitoring is vital to identify hotspots of groundwater exploitation, analyze aquifer characteristics at higher resolution and prepare precautionary and mitigatory measures for impending groundwater-related hazards.

## 1. Introduction

Vertical lowering of the land surface (subsidence) induced by natural and anthropogenic processes is a widespread phenomenon (Riyas et al., 2021; Fernandez et al., 2018; Higgins et al., 2014; Fielding et al., 1998). While natural causes can vary broadly, land subsidence due to over-exploitation of groundwater aquifers is evident worldwide (Herrera-García et al., 2021). In the case of groundwater, extraction of water leads to a reduction in pore pressure and subsequent increase in vertical stress leading to lowering of the land surface (Terzaghi, 1925). With the increasing dependency of the human population on groundwater reserves, land subsidence will reach hazardous proportions with the

potential to cause immense damage to civil infrastructure (Carlson et al., 2020; Shirzaei and Bürgmann, 2018). Realizing the adverse impact of anthropogenic land subsidence on Sustainable Development Goals (SDG), UNESCO International Hydrological Program VIII (2014–20) has emphasized its regular reporting and monitoring at a global scale (UNESCO, 2017).

Spaceborne Interferometric Synthetic Aperture Radar (InSAR) has emerged as an effective, rapid, and cost-effective technique for measuring land subsidence at spatial resolutions of few meters and temporal resolution of days to months (Simons and Rosen, 2007). In recent times, InSAR techniques have been utilized to study land subsidence, due to excessive groundwater extraction, in some of the major

\* Corresponding author.

E-mail address: [tsyed@iitk.ac.in](mailto:tsyed@iitk.ac.in) (T.H. Syed).

cities in the world (Miller et al., 2017; Miller and Shirzaei, 2015; Erban et al., 2014; Cigna et al., 2012; Chatterjee et al., 2006; Amelung et al., 1999). Apart from monitoring land subsidence associated with aquifer system compaction, InSAR-based measurements of subsidence have helped identify groundwater flow barrier, aquifer extent, and mapping of recharge areas (e.g. Hu et al., 2018; Hoffmann et al., 2003; Bawden et al., 2001; Lu and Danksin, 2001; Amelung et al., 1999). Additionally, time series of surface deformation has enabled the analysis of subsidence and subsequent recovery during or post-drought events (Murray and Lohman, 2018), characterization of the poroelastic response of aquifers to artificial recharge (Miller and Shirzaei, 2015; Chaussard et al., 2014), nature of aquifer deformation (Ezquerro et al., 2014), estimation of aquifer storage parameters and prediction of the hydraulic head (Chen et al., 2016; Chaussard et al., 2014; Reeves et al., 2014). However, such estimates, particularly aquifer storage parameters, require concurrent groundwater level and subsidence data, which unfortunately is not available in most data-scarce parts of the world, including the study area. Recent studies have shown potentials for the integrated use of InSAR and Gravity Recovery and Climate Experiment (GRACE) datasets for supporting and assessing groundwater management practices (e.g., Castellazzi et al., 2017; Castellazzi et al., 2016).

National Capital Region (NCR) of India is a very rapidly developing urban conglomerate and has a population of 46.1 million, according to the 2011 census estimate. The requirement of water for domestic and industrial usage has created enormous pressure on groundwater resources and has already stressed the aquifer system. Previous studies based on Gravity Recovery and Climate Experiment (GRACE) satellites had shown alarming levels of groundwater depletion in North-western India and Indo-Gangetic plain, including Delhi and surroundings areas (Soni and Syed, 2015; Rodell et al., 2009; Tiwari et al., 2009). While these regional studies are very effective for overall resource assessment, it lacks the spatial resolve to isolate small-scale heterogeneities which are crucial for identifying hot spots and sustainable groundwater development. Hence, InSAR-based monitoring of land subsidence due to groundwater extraction can form the basis for actionable information required to monitor and regulate groundwater resources by water managers and stakeholders.

Although InSAR has been widely used to characterize surface deformation due to groundwater extraction in several parts of the world, such detailed studies are very limited in the Indian context. Those that exists are more primarily focussed on the identification of subsidence zones (e.g. Suganthi and Elango, 2020; Chatterjee et al., 2006) and do not investigate the temporal evolution and nature of deformation in response to groundwater extraction. In the present study, we use InSAR to measure the time series of vertical displacement in NCR, over the periods of 2007–10 and Nov. 2014–19, to identify regions most significantly affected by subsidence. These deformation estimates are analyzed in the context of limited observations of groundwater level to ascertain the causes of subsidence and their spatiotemporal variations. Further, we study the temporal behaviour of surface deformation during Nov. 2014–19 to characterize the nature of aquifer deformation.

## 2. Study area

The study area is part of the Indo-Gangetic alluvial plain (Fig. 1) and drained by the Yamuna River, which flows from northwest to southeast following the natural slope of 0.4 m/km. Elevation of the region varies from ~ 205 m in flood plains of Yamuna river to 250 m in parts of Delhi ridge. The area receives a majority of the rainfall (81%) during the monsoon period (July - September), while the rest of the rainfall is spread throughout the year.

Physiographically, the study area can be divided into four major geomorphic units: (i) Delhi ridge, (ii) alluvial plains on the eastern and western side of the ridge, (iii) Yamuna floodplains and, (iv) Chattarpur alluvial basin (Kaul and Pandit, 2004). The Delhi ridge, a regional coaxially folded anticlinal structure is plunging southeast, consists of

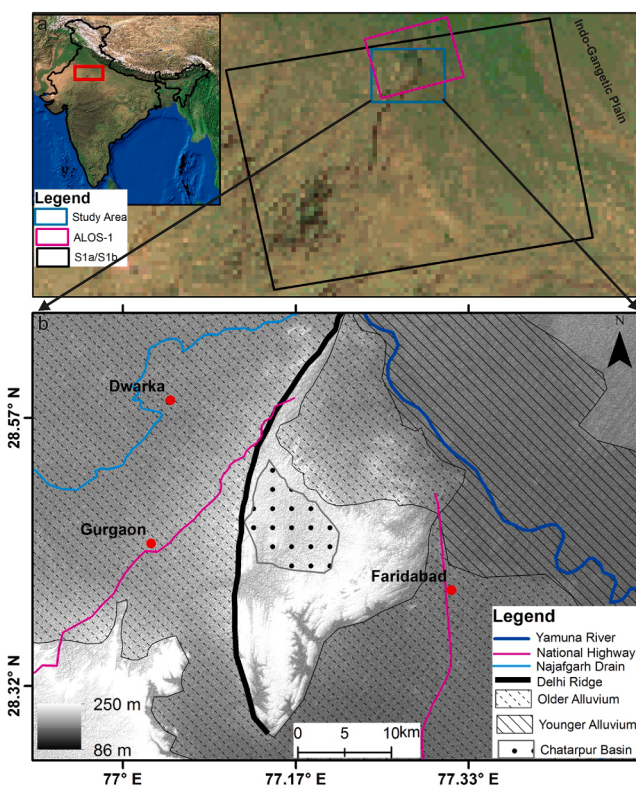


**Fig. 1.** (a) Location map of study area. Data coverage of ALOS-1 and Sentinel-1 satellites are overlaid. (b) Different physiographic/hydrogeomorphic units (younger alluvium, older alluvium, Chattarpur alluvial basin and Delhi ridge) are overlaid on SRTM DEM. Road network, major drainage and locations are marked for reference.

fractured quartzites of the Proterozoic era with interbedded mica schists and acts as a basement (CGWB, 2006). On the western and eastern side of the ridge, older alluviums are present, while younger alluvium occupies the flood plains of Yamuna River. The Chattarpur alluvial basin located on the eastern part of the ridge is a closed alluvial basin and consists of alluvium derived from the adjacent ridge. The Delhi ridge acts as a major watershed divide, and runoff generated east of ridge drains to the Yamuna River, while runoff generated on the western side is directed towards regional depressions.

The occurrence of groundwater is mainly limited to alluvial aquifers. Two major water-bearing horizons comprising of coarse-grained sand and kankar (local name for calcareous concretions mixed small gravels) occur at 30–35 and 115–120 m below ground level (mbgl) in older alluviums (Chatterjee et al., 2009). In Chattarpur alluvial basin, bed rock (quartzite) is overlain by silt, clay and varying proportion of kankar. The water bearing horizons occur at 20–35, 30–70 and 80–115 mbgl in this basin. In flood plains of Yamuna river (younger alluvium) the water bearing horizons are located at 30–65 mbgl. The unconfined aquifer system extends up to 60 mbgl while the deeper confined to semi-confined aquifer systems are characterized by the presence of sand layer at 65 to more than 300 mbgl (CGWB, 2012). Aquifer systems underlain by older alluvium are dominated by clay and mixed with sand, silt, and kankar, while sand admixed with silt, clay, and gravel dominates the aquifer system of younger alluvium (Shekhar and Prasad, 2009). Groundwater levels in aquifers are monitored by ground-based network of observation wells and are limited to shallow, unconfined, and semi-confined aquifer systems (CGWB, 2016a). However, the confined aquifers located at depths greater than 200 m are largely unmonitored by the existing network.

### 3. Data and methodology

#### 3.1. Datasets

To study surface deformation of NCR using the InSAR, a total of fifteen scenes of L-band ALOS PALSAR ( $\lambda = 23.6$  cm, incidence angle =  $34.1^\circ$ ) spanning the period 2007–10 acquired during descending pass are used. Datasets (116 scenes) from Sentinel-1 series of satellites ( $\lambda = 5.54$  cm, incidence angle =  $37.5^\circ$ ) acquired during descending pass spanning Nov. 2014–2019 are used to understand the spatial and temporal evolution of subsidence zones.

Groundwater level data for observation wells are obtained from Water Resource Information System (WRIS) (<https://indiawris.gov.in/wris/#/>) web portal. Groundwater level readings are acquired four times a year (January, May, August, and November).

#### 3.2. Multi-temporal InSAR analysis

InSAR processing uses coherent radar signals of the same area, acquired at different periods, to derive high-resolution surface deformation estimates along the line of sight (LOS) of the satellite (Simons and Rosen, 2007). As a part of InSAR processing, a stack of coregistered multi-looked interferograms are generated from an ensemble of SAR scenes using the ISCE software (Rosen et al., 2012). Topographic phase contributions modeled using Shuttle Radar Topographic Mission (SRTM) digital elevation model (Farr et al., 2007) are removed from each interferogram. Random phase noise of the interferograms is reduced using an adaptive phase filter (Goldstein and Werner, 1998), and the resulting interferograms are then phase unwrapped using Statistical-cost, Network-flow Algorithm for PHase Unwrapping (SNAPHU) tool (Chen and Zebker, 2000).

Time series of surface deformation at the pixel level is computed using the Miami InSAR Time series software in Python (MintPy) (Yunjun et al., 2019). This software integrates a large number of interferograms using the Small Baseline Subset (SBAS) technique (Doin et al., 2011; Berardino et al., 2002). The SBAS technique enables a detailed analysis of the temporal evolution of deformation in an area. The technique integrates a large number of multilooked unwrapped interferograms, which are separated by short temporal and spatial baseline to retrieve the time series of surface deformation (Usai, 2003; Lundgren et al., 2001). The tropospheric contributions in interferograms (for both ALOS-1 and Sentinel-1) due to vertical stratification and turbulent mixing are reduced by computing the path delays from ERA5 (European Centre for Medium Range Weather Forecasts) model (Hersbach et al., 2020)). The reference pixel is selected within the region, which showed high temporal coherence ( $>0.85$ ), located in a stable area and at the same elevation as the area of interest, and is not strongly affected by troposphere and ionosphere-induced path delays. Phase ramps caused by topographic residuals, orbital error and remaining atmospheric contributions are removed by fitting quadratic and linear ramps for ALOS-1 and Sentinel-1, respectively. The phase due to errors in the digital elevation model is directly proportional to the perpendicular baseline history of the SAR acquisitions, which introduces biases in the time series of deformation. This bias is corrected by modelling the phase due to errors in the digital elevation model in temporal domain utilizing phase velocity history (Fattah and Amelung, 2013). ALOS-1 interferograms exceeding the perpendicular baseline of  $\sim 2.5$  km, which is approximately half the critical baseline, are not included in the analysis as they may lead to geometrical decorrelation. The perpendicular baseline for all the Sentinel-1 interferograms ( $<200$  m) is well under the critical perpendicular baseline requirement for C-band. Finally, after discarding the interferograms based on perpendicular baselines, we use 106 and 475 interferograms generated from ALOS-1 and Sentinel-1 scenes, respectively, to generate surface deformation time series at 90-meter spatial resolution. The temporal coherence of 0.7 is used to avoid the pixels with unwrapping errors.

The derived surface displacement is sensitive to Line of Sight (LOS) of the satellite and is referred to as LOS displacement. However, polar-orbiting satellites are not sensitive to the north–south component of surface displacement, and there is no evidence of significant east–west displacement in the study area. Hence, LOS displacements obtained earlier are converted to vertical displacement by dividing it by the cosine of incidence angle. It is to be noted that ALOS-1 and Sentinel-1 surface displacement time series could not be connected as they do not share any common time period. Average vertical velocity is computed by dividing the cumulative vertical displacement with the temporal duration of datasets. Since ground-based measurements are not available for our study area, we cannot quantify the uncertainty in our deformation estimates. Instead, we compute a pseudo-uncertainty estimate by evaluating the standard deviation of vertical displacement observed in pixels located within a radius of  $\sim 3$  km of relatively stable regions (located away from known subsidence zones). Our estimate of pseudo-uncertainty in subsidence values obtained from ALOS-1 is 1.46 cm/year and for those derived using Sentinel-1 dataset is 1.15 cm/year. These pseudo-uncertainty estimates are also in close agreement with those in previous studies conducted elsewhere (e.g., Smith and Li, 2021).

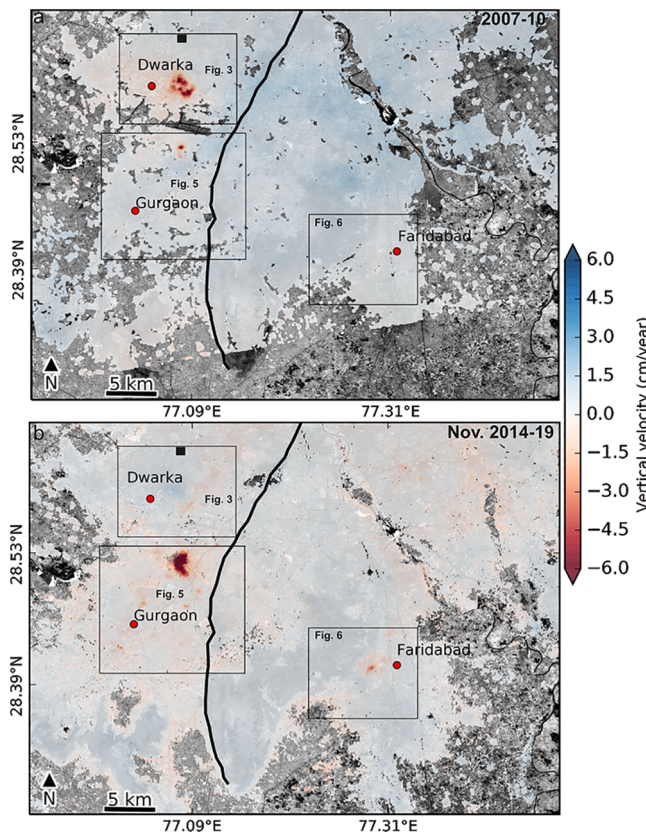


**Fig. 2.** (a) Vertical velocity map (cm/year) derived from ALOS-1 datasets of 2007–10 and (b) Sentinel-1 datasets of Nov. 2014–19 using SBAS technique. Time series of vertical displacements are referenced to region marked in solid rectangle, north of Dwarka in (a) and (b). Two major subsidence zones located in vicinity of Dwarka and Gurgaon are detected during 2007–10. The spatial extent of these two subsidence zones and a newly developed subsidence zone near Faridabad during Nov. 2014–19 (b). Spatial and temporal evolution of subsidence zones marked in rectangles (Figs. 3, 5 and 6) are discussed. Delhi ridge (black coloured line) is overlaid on vertical velocity map.

## 4. Results

### 4.1. Vertical displacement of land surface

Shown in Fig. 2 are the rates of vertical displacement (vertical velocity in cm/year) derived from ALOS-1 (a) and Sentinel-1 (b) datasets for the period 2007–10 and Nov. 2014–19, respectively. By convention, negative values of vertical velocity depicts the rate at which subsidence occurs, shown in shades of red. Upliftment zones (positive vertical velocity) are shown in shades of blue. Regions outside the sharply defined subsidence zones (seen in lighter shades) show inconsiderable vertical velocity ranging between −0.78 to +1.2 cm/year, which are within the pseudo-uncertainty estimated for ALOS-1 ( $\pm 1.46$  cm/year) and Sentinel-1 ( $\pm 1.15$  cm/year). Such small vertical velocities are most likely caused by spatiotemporal variations in scattering properties of surfaces and residual atmospheric artifacts, introducing errors in the range  $\pm 0.5$ – $1.0$  cm/year (Erban et al., 2014). Here we assume the

regions within our pseudo-uncertainty estimate to be nearly stable. The areas devoid of any displacement measurements are regions where temporal correlation is lost due to changing land cover/vegetation types.

During the period 2007–10, two prominent subsidence zones, located east of Dwarka and around Gurgaon are seen in Fig. 2a. The subsidence zone near Dwarka is approximately  $\sim 4$  km long and  $\sim 3$  km wide, with vertical velocities varying between  $-2.5$  and  $-6.0$  cm/year. The subsidence zone near Gurgaon is of a relatively smaller dimension ( $\sim 1$  km  $\times$  1 km) but shows an equally high vertical velocity of  $-1.5$  to  $-6.0$  cm/year.

Between Nov. 2014–19, the spatial extent of the subsidence zone near Dwarka reduced to  $\sim 2.5 \times 2.5$  km and concomitantly its vertical velocity (ranging from  $-1.5$  to  $-2.0$  cm/year). Contrastingly, the subsidence zone in Gurgaon expanded to  $\sim 3$  km  $\times$  4 km in dimension, and the velocity also increased significantly to about  $-1.6$  to  $-11.5$  cm/year. The other minor subsidence zones located in the vicinity of Gurgaon are

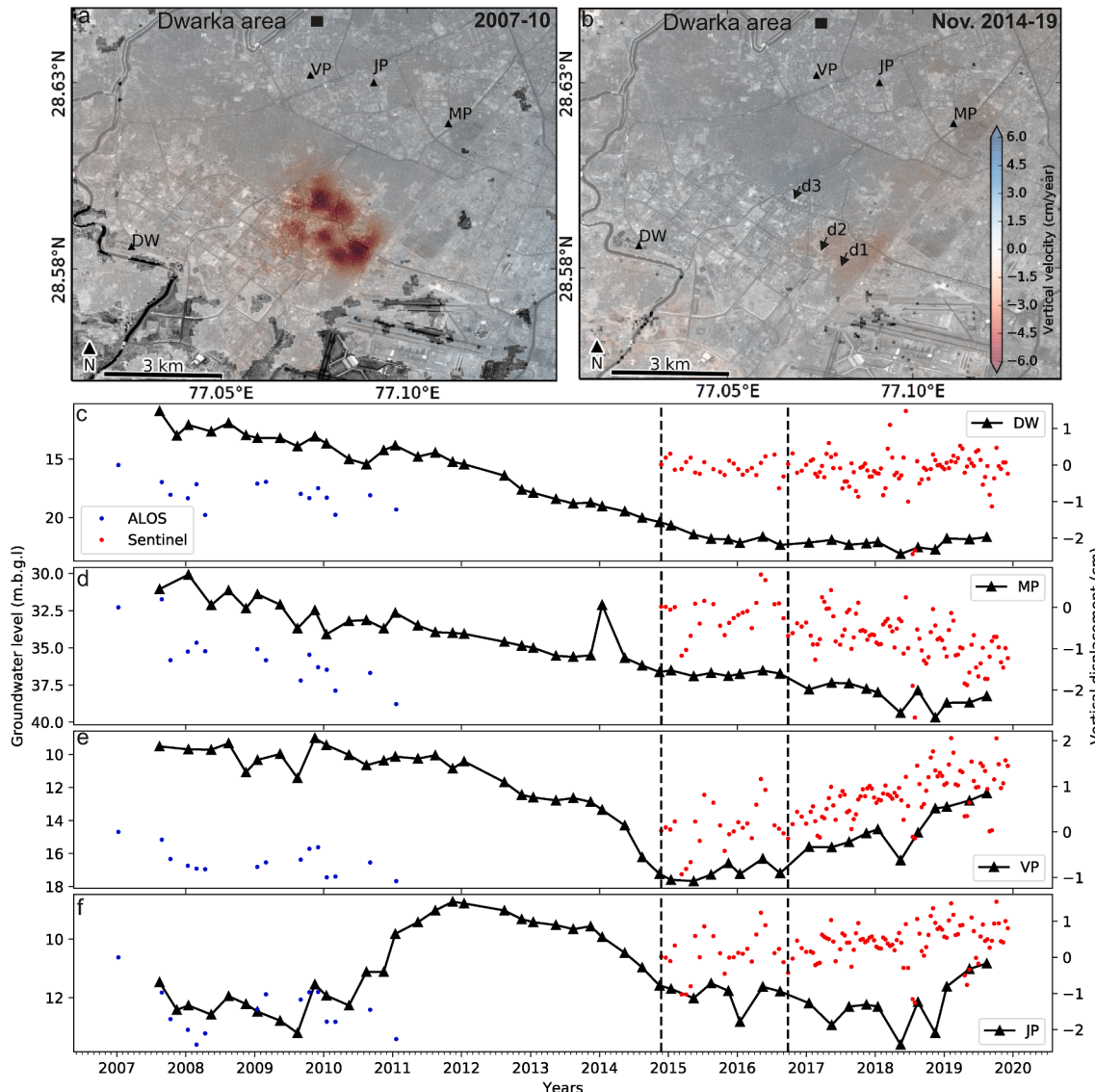


**Fig. 3.** (a) Subsidence zones in Dwarka area during 2007–10 and (b) Nov. 2014–19 overlaid on band 3 of Sentinel-2. Reference area (black coloured solid rectangle) is overlaid. Locations of groundwater observation wells Dwarka (DW), Mayapuri (MP), Vikaspuri (VP) and Janakpuri (JP) are overlaid. Also shown is the inter-comparison of groundwater level (black line) and vertical displacement time series from ALOS-1 (blue dots) and Sentinel-1 (red dots) around each of the observation wells Dwarka (c), Mayapuri (d), Vikaspuri (e) and Janakpuri (f). Two vertical dotted black coloured lines are located at Nov. 2014 and Sept. 2016. Time series of vertical displacement of points d1, d2 and d3 marked on (b) are shown in Fig. 4a. (For interpretation of the references to colour in this figure legend, the reader is referred to the web version of this article.)

relatively smaller ( $\sim 1.0 \text{ km} \times 1.0 \text{ km}$ ) in size and show vertical velocity in the range of  $-2.0$  to  $-5.5 \text{ cm/year}$ . The subsidence zone near Faridabad has an expanse of  $\sim 3 \times 1.5 \text{ km}$  with vertical velocities ranging from  $-1.6$  to  $-3.6 \text{ cm/year}$ . In the following sections, the causative factors, spatiotemporal variations, and nature of subsidence are discussed for each of these subsidence zones.

#### 4.2. Analysis of subsidence in Dwarka area

##### 4.2.1. Vertical displacement versus groundwater level

In order to ascertain the causative factors of subsidence, we analyze groundwater level datasets. Shown in Fig. 3a and b are the locations of groundwater observation wells in the vicinity of the noted subsidence zones for the period 2007–2019. Since no groundwater observation well is located within the zones of maximum subsidence, analysis of groundwater level and corresponding vertical displacement is limited to observation wells located in the proximity of subsidence zones. Fig. 3 (c–f) shows the time series of groundwater level measurements for the observation wells at Dwarka (DW) (c), Mayapuri (MP) (d), and Vikaspuri (VP) (e) and Janakpuri (JP) (f). The vertical displacement from ALOS-1 and Sentinel-1 corresponding to 2007–10 and Nov. 2014–19 are also shown. Here, vertical displacement around each observation well is calculated as the average displacement value of all the pixels lying within a 500 m radius of the observation well. This approach is adopted for all the inter-comparisons between groundwater level and vertical displacement discussed in the subsequent sections.

To quantitatively assess the relationship between groundwater level and vertical displacement, we interpolate the groundwater level measurements to time stamps at which vertical displacement estimates are available. Correlation coefficients computed for temporally collocated groundwater level and vertical displacement show the highest value for Mayapuri (0.68) followed by Dwarka (0.55), Janakpuri (0.53), and Vikaspuri (0.32) ( $p\text{-value} < 0.05$  for all the wells) for the period 2007–10 (ALOS-1 observation period). During Nov. 2014–19 (Sentinel-1 observation period), the highest value of correlation coefficient is noted for Mayapuri (0.77) followed by Dwarka (0.75), Vikaspuri (0.58), and Janakpuri (0.24) with a  $p\text{-value} < 0.05$ . For both the observation periods (2007–10 and Nov. 2014–19), the deeper wells (Mayapuri and Dwarka), in which groundwater level varies between 18 and 40 m bgl, show a higher correlation compared to the shallower wells. The observation well Vikaspuri shows poor correlation during 2007–10 when groundwater was shallow ( $\sim 10 \text{ m}$  bgl). However, the correlation improved during Nov. 2014–19, wherein groundwater level dropped up to 18 m bgl. Hence, the average correlation coefficient between groundwater level and vertical displacement is significantly higher (0.72) for relatively deeper wells (such as Dwarka and Mayapuri) in comparison to shallower wells (0.28). These observations suggest that the observed subsidence zones may be related to groundwater pumping from relatively deeper levels of the earth's subsurface.

As noted earlier, the spatial extent of subsidence zones near Dwarka shows a marked difference between 2007–10 and Nov. 2014–19. The plausible cause of the reduction in magnitude and extent of subsidence zone during Nov. 2014–19 is investigated by computing the rates of groundwater level fluctuation in each well for 2007–14 and Nov. 2014–19. Further, the same can be used to compare the pre-and post-Nov. 2014 changes in groundwater level trend. The three observation wells Dwarka, Mayapuri, and Vikaspuri show a decline in groundwater level at a rate of  $-1.15$ ,  $-0.66$ , and  $-0.78 \text{ m/year}$  (negative sign for declining groundwater level), respectively, for the period 2007–14. During Nov. 2014–19, groundwater level declined at a reduced rate in Dwarka ( $-0.42 \text{ m/year}$ ), and Mayapuri ( $-0.33 \text{ m/year}$ ), while in Vikaspuri, the groundwater level shows an increasing trend ( $1 \text{ m/year}$ ). Given the limitations mentioned earlier, we consider the trend in groundwater levels of nearby monitoring wells to represent the general trend of groundwater level in and around the subsidence zone. Based on this consideration, we can infer that reduction in the rate of

groundwater level decline post-Nov. 2014 as the most probable cause for the prominent decrease in the spatial extent as well as in the magnitude of subsidence in the Dwarka area.

##### 4.2.2. Time series vertical displacement

Dense time series datasets available from Sentinel-1 for Nov. 2014–19 are investigated to understand the temporal behavior of vertical displacement for the subsidence zone near Dwarka. Marked in Fig. 3b are the locations of the sample points considered for the study of temporal variations in vertical displacement (Fig. 4a). The temporal profiles for all the points d1, d2, and d3 representing the lower, and middle and upper parts of the subsidence zone show a rapid declining trend until Sept. 2016. Subsequently, a clear upward trend is noted for d2 and d3, while point d1 shows signs of stabilization. This complex non-linear temporal behavior of vertical displacement is modelled by fitting two linear models.

The slope of first linear model captures the declining trend of vertical displacement until Sept. 2016, while the second one models the stabilizing/upward trend as observed in the temporal profiles after Sept. 2016. Also evident are significant variations in the spatio-temporal pattern of vertical displacement within the subsidence zones (Fig. 4b and c). For example, the lowermost part of the subsidence zone (Fig. 4b) shows a vertical velocity of  $\sim -6.5 \text{ cm/year}$  until Sept. 2016, which stabilized after Sept. 2016. On the contrary, the uppermost region, which shows moderate subsidence with velocity reaching up to  $-3.25 \text{ cm/year}$  until Sept. 2016 (Fig. 4b), shows feeble upliftment (1 cm/year) (Fig. 4c) after Sept. 2016. Although the groundwater level in nearby observation wells shows stabilizing trend post-2014, the continuation of subsidence until Sept. 2016 can be attributed to equilibration of hydraulic heads of aquifers with neighboring aquitard units. Groundwater extraction leads to a differential decline in pore pressure in the underlying aquifer and overlying aquitard units, which leads to the development of a hydraulic gradient between the aquitard and aquifer units. Hence, subsidence continues till an equilibrium is attained between the aquifer and aquitard units, a process known as residual compaction (Ojha et al., 2020; Bell et al., 2008).

#### 4.3. Analysis of subsidence in Gurgaon area

The subsidence zone near Gurgaon, which has a relatively smaller spatial extent ( $\sim 1 \text{ km} \times 1 \text{ km}$ ) during the 2007–10 time period (Fig. 5a), show a significant enlargement ( $2.5 \text{ km} \times 3.5 \text{ km}$ ) in extent between Nov. 2014–19 (Fig. 5b). This increase in spatial extent is also accompanied by an enhanced subsidence rate, which increased by an average of  $\sim 4 \text{ cm/year}$  during the entire study period. Apart from the existing subsidence zones, few emerging but prominent, subsidence zones (located south of the major subsidence zone) of relatively smaller ( $\sim 1.0 \times 1.0 \text{ km}$ ) spatial extent and vertical velocity ( $-2.0$  to  $-4.5 \text{ cm/year}$ ) are also noted. The relationship between vertical displacement and groundwater level variations is studied for the GU well since no observation well is located within the subsidence zone (Fig. 5b). Groundwater level observations are relatively stable during 2007–10 (ALOS-1 observation period), which is also reflected in vertical displacements estimates using ALOS-1 (Fig. 5c). After 2014, a steady decline of  $\sim 2 \text{ m/year}$  in groundwater level is noted, which is replicated to a certain degree by the vertical displacement measured using Sentinel-1. The trend estimate for vertical displacement for Nov. 2014–19 is  $-0.2 \text{ cm/year}$ . Overall, the fluctuations in groundwater level and time series of vertical displacement are in good agreement suggesting groundwater extraction as the primary cause of subsidence.

The time series of vertical displacement for two representative points located at the center (g1) and periphery (g2) of the subsidence zone is shown in Fig. 5d. The cumulative magnitude of vertical displacement reaches up to  $-45 \text{ cm}$  and  $-11 \text{ cm}$  for the central and peripheral parts, respectively, during Nov. 2014–19. Both the temporal profiles show linear variations in vertical displacement. To assess the presence of

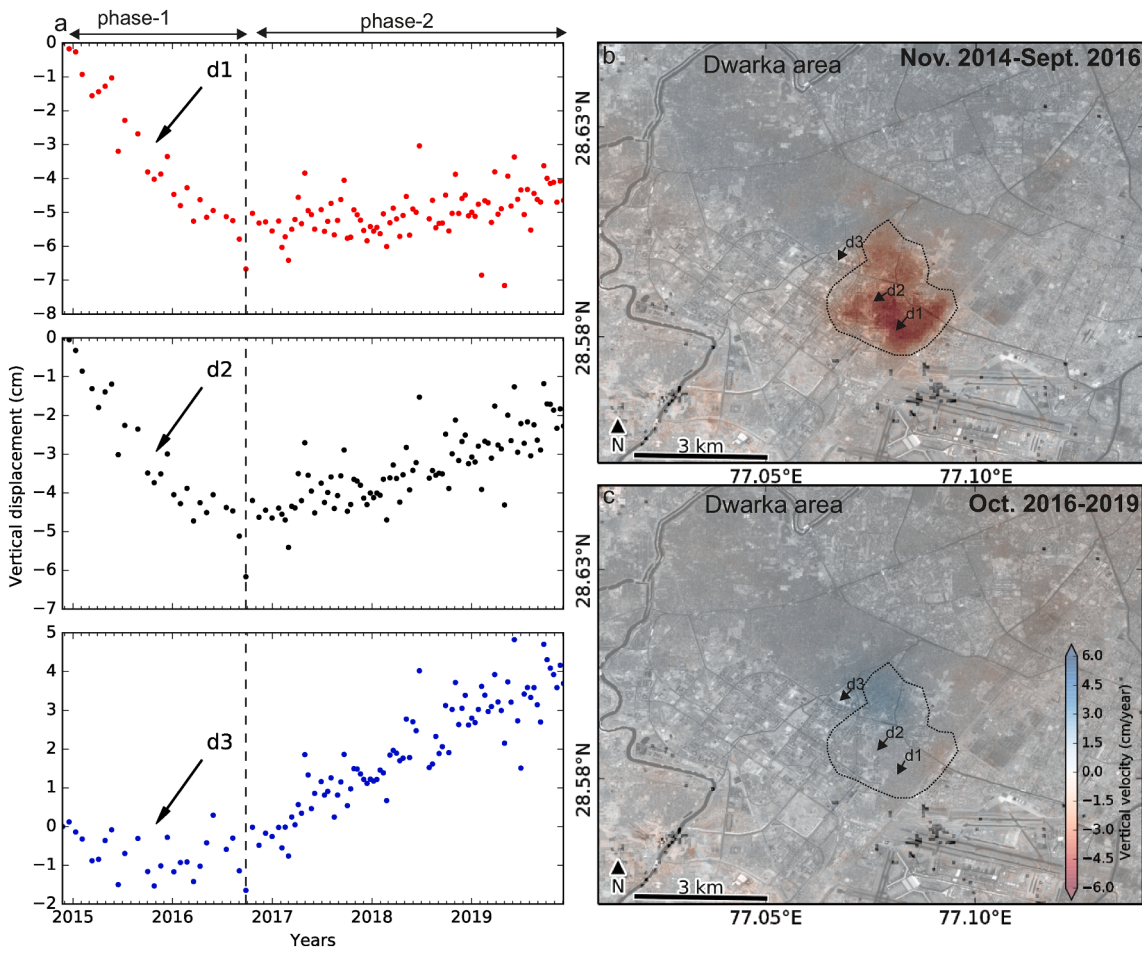


**Fig. 4.** (a) Time series of vertical displacement of locations (d1, d2 and d3) marked in Fig. 3b for time period Nov. 2014–19. Two distinct temporal behaviour (i) phase-1 (fast subsidence) and (ii) phase-2 (stable/recovery of subsidence) is delineated. Dotted black coloured line is placed at time stamp Sept. 2016. (b) Vertical velocity between Nov. 2014–Sept. 2016 and (c) Oct. 2016–19 corresponding to phase-1 and phase-2 is estimated. Black coloured polygon represents the extent of subsidence zone between Nov. 2014 – Sept. 2016.

seasonality in the time series, we fit two functions, one having only linear terms ( $at + c$ ) and the other with both linear and seasonal terms ( $at + Asin(2\pi t) + Bcos(2\pi t) + c$ ). Here,  $a$  is the slope of the linear model,  $t$  represents time,  $\sqrt{A^2 + B^2}$  is the amplitude of the seasonal signal and  $c$  accounts for constant shift in model due interferometric noises and artifacts. The latter model, consisting of both seasonal and linear terms, shows a decrease in residuals compared to the linear model, but this may be due to more number of free parameters. Subsequently, an ‘F-test’ statistic (Menke, 2018; González and Fernández, 2011) is computed to check whether the decrease in residuals is due to fitting of noise in the data or an accurate representation of inherent variability. The F-test shows that the decrease in residual due to the addition of seasonal term is not statistically significant. This result indicates that the seasonal signals cannot be distinguished from noise in the vertical displacement time series. Further, isolating low amplitude (order of few mm) seasonal signals from residual tropospheric noise is challenging in the study area as the timing of recharge, primarily during the monsoon period (June–September), is coincident with high water vapor variability in the troposphere above the study area. Therefore, we assume that there are no significant seasonal signals. The dominance of linear variation clearly indicates continuous groundwater extraction and consequent inelastic deformation.

#### 4.4. Analysis of subsidence in Faridabad area

During 2007–10, no significant subsidence is observed around

Faridabad (Fig. 6a). However, after Nov. 2014, a major subsidence zone with a vertical velocity ranging from  $-1.65$  to  $-3.6$  cm/year is observed over an extent of  $\sim 3$  km  $\times$  1.5 km. Since no observation well exists within the subsidence zone, groundwater level measurements and collocated time series of vertical displacement available for a nearby observation well (P1) are studied (Fig. 6b and c). Time series of groundwater levels indicate that the area has witnessed a steady decline of groundwater level till 2014. The time series of vertical displacement is not available for 2007–10 (ALOS time period) due to loss of coherence, thus hindering its analysis with groundwater level. Post-2014, groundwater level declined in P1 at a very steep rate (8 m/year) and is fairly manifested in the collocated time series of vertical displacement obtained from Sentinel-1 for Nov. 2014–19 (Fig. 6c). Time series of vertical displacement derived from Sentinel-1 for the regions surrounding the two representative points located at the center (f1) and periphery (f2) of the subsidence zone is shown in Fig. 6d. The magnitude of cumulative vertical displacement during the five years is  $-7$  cm and  $-1.5$  cm for f1 and f2 respectively. Here also, similar to Gurgaon, the temporal profiles clearly show a linear progression of deformation and the lack of significant seasonal effect indicating inelastic deformation of the aquifer system.

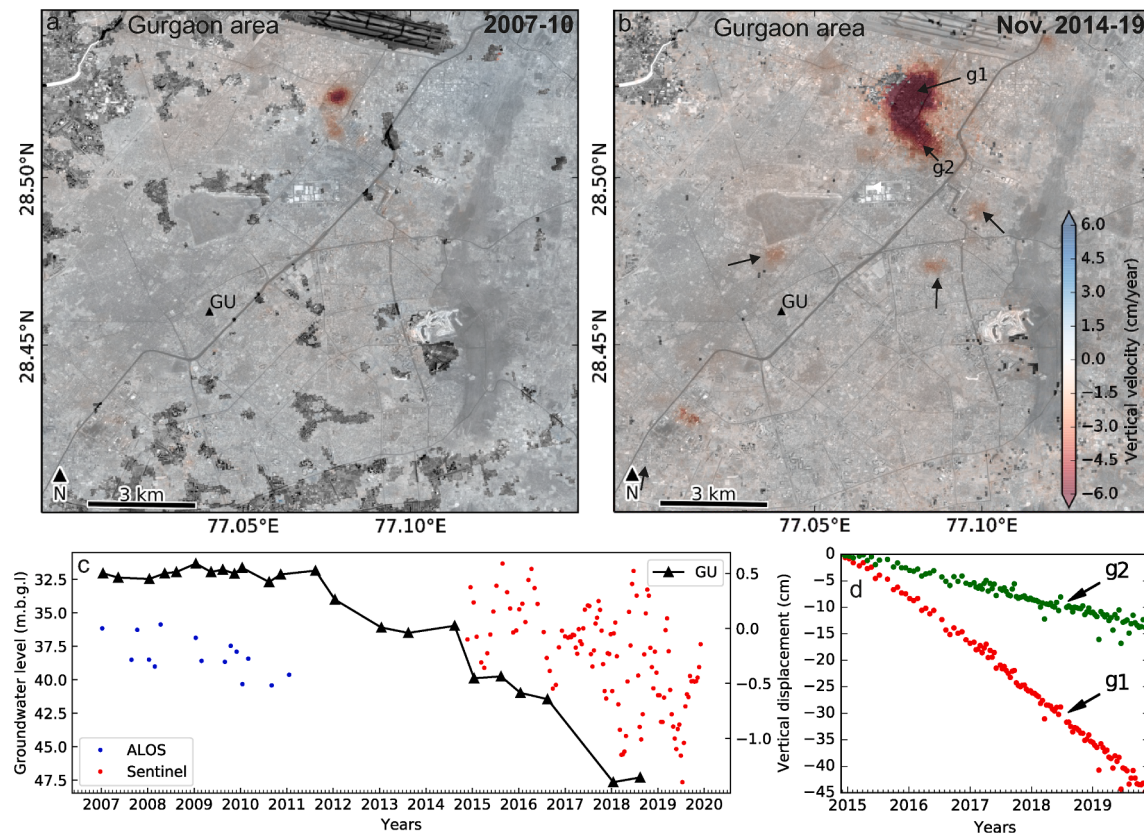


**Fig. 5.** (a) Subsidence zones near Gurgaon during time period 2007–10 and (b) Nov. 2014–19. New emerging subsidence zones (post Nov. 2014) in vicinity of Gurgaon are marked by black coloured arrows (b). Location of groundwater observation well GU is overlaid. (c) Intercomparison of time series of vertical displacement and groundwater level datasets for observation well GU. (d) Time series of vertical displacement for locations (g1 and g2) marked in (b).

## 5. Discussions

### 5.1. Subsidence caused by groundwater extraction

The rapid subsidence observed in this study area cannot be attributed to natural compaction. The subsidence rate (negative vertical velocity) due to natural compaction (due to superincumbent pressure) is only in the order of a few mm/year (Teatini et al., 2011). In addition, the rates and spatial distribution of subsidence shown here correlate well with the observed patterns of declining/stabilizing groundwater levels. Therefore, we can conclude that groundwater extraction for domestic (meet the requirement of urban population) and industrial purposes is the primary cause of land subsidence observed here.

### 5.2. Mechanism of subsidence

There exist strong links between groundwater extraction and surface subsidence both in terms of trend and spatial distributions. The vertical displacement due to fluctuations in the hydraulic head is explained by the aquitard-drainage model (Chaussard et al., 2014). Lowering of hydraulic head in a confined aquifer leads to a decrease in pore pressure in the aquifer system and a proportional increase in effective vertical stress, which leads to subsidence. The mechanism of land surface subsidence caused by groundwater may vary from place to place owing to variations in groundwater pumping rate, natural recharge, the thickness of compressible materials, and pre-consolidation stress. During 2007–10, the subsidence zone in the Dwarka region was mainly due to excessive groundwater extraction. However, the subsidence halted during Nov. 2014–19 time frame in response to the stabilization of groundwater levels. Similarly, the steep decline in groundwater level during Nov. 2014–19 in the Gurgaon region led to increased subsidence

rate and enlargement of subsidence zone compared to its magnitude and extent in 2007–10. In the wake of declining groundwater levels after 2014, a new subsidence zone is also detected west of Faridabad. It is also important to note that the subsidence and decline in groundwater levels do not show any time lag in Gurgaon and Faridabad.

In the Dwarka region, the subsidence continued till Sept. 2016 even after no appreciable decline in groundwater level is noted in the nearby observation wells (Fig. 3c-f). In fact, during Nov. 2014–16, these observation wells show signs of stabilization in groundwater levels. Thus, the rapid subsidence in Dwarka, which continued till Sept. 2016, maybe due to residual or delayed compaction experienced by the aquifer system even after the groundwater levels have stopped declining (Shirzaei et al., 2019; Miller et al., 2017). This behavior occurs due to the equilibration of the hydraulic head in the aquifer and neighboring aquitard units (Smith et al., 2017). The time taken for the equilibration and subsequent termination of subsidence depends mainly on the hydraulic conductivity and thickness of aquitard units (Schmidt and Bürgmann, 2003). Delayed compaction as a major cause of transient non-linear behavior of subsidence was also reported earlier by Miller et al. (2017), Shirzaei, et al., (2017) and González and Fernández (2011). The possibility that groundwater extraction and halting of subsidence are coterminous is improbable since the region is dominated by clay layers (CGWB, 2016b). Hence, instant equilibration of aquifer hydraulic head with neighbouring aquitard units seems implausible. That residual compaction ceased post-Sept. 2016, and vertical displacement estimates are either stabilizing or revealing trends of upliftment, suggests that the inelastic deformation phase is over, and the underlying aquifer is behaving elastically at present.

In contrast to the non-linear temporal behavior of the subsidence region in Dwarka, the subsidence zones of the Gurgaon and Faridabad region show a dominantly linear behavior with a negligible seasonal

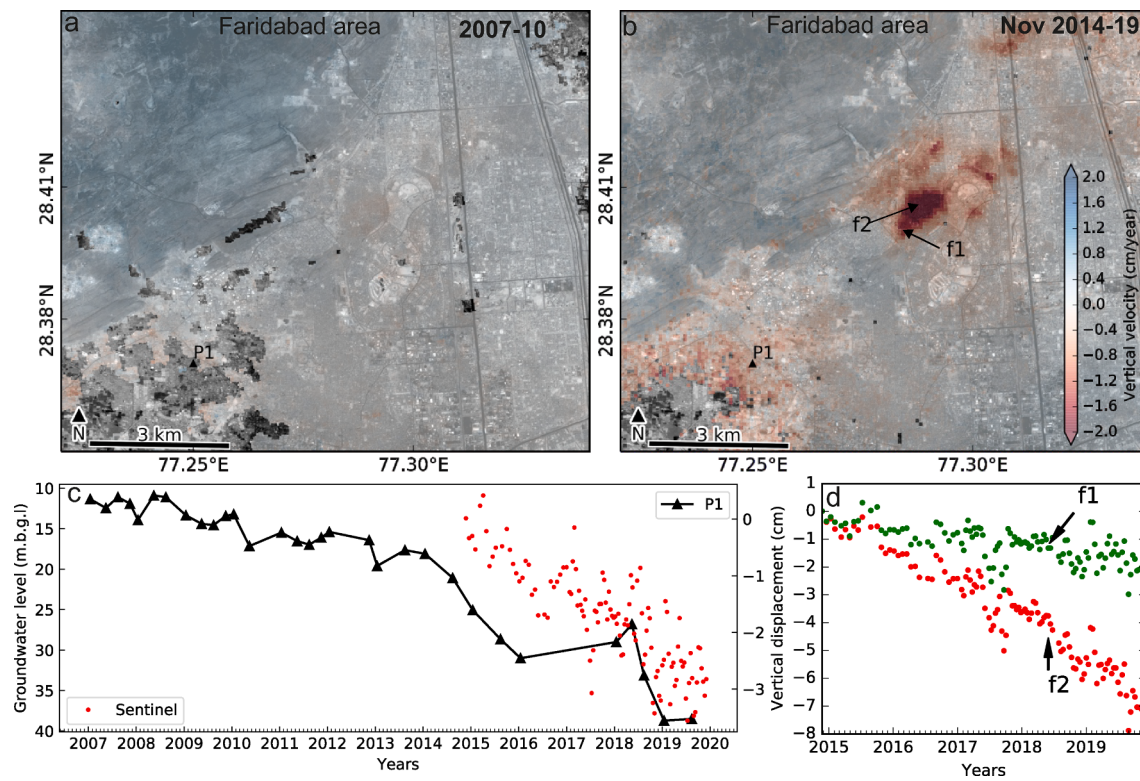


**Fig. 6.** (a) Vertical velocity (cm/year) in and around Faridabad during 2007–10 and (b) Nov. 2014–19. No obvious subsidence is seen during 2007–10 (a). Newly developed subsidence zones near Faridabad during time period Nov. 2014–19 (b). Location of groundwater observation well P1 is overlaid. (c) Intercomparison of vertical displacement and groundwater level datasets for observation well P1. (d) Time series of vertical displacement for locations (f1 and f2) marked in (b).

component. Long-term records of groundwater level from existing monitoring wells show the lowest values of groundwater level since the start of monitoring, suggesting inelastic deformation of the aquifer system. This type of deformation invariably leads to non-reversible rearrangement of grains (Wilson and Gorelick, 1996) and permanent loss of aquifer storage (Smith and Knight, 2019; Chaussard et al., 2014; Hoffmann et al., 2003; Poland and Ireland, 1988). Processes like this have serious consequences for freshwater water availability and compel immediate supply or demand-side interventions to restrict the aquifer deformation to elastic range only (Chaussard et al., 2017; Bell et al., 2008; Hoffmann et al., 2001).

### 5.3. Compartmentalisation of aquifer system

The major subsidence zones near Dwarka, Gurgaon, and several minor and emerging subsidence zones, are located on the western side of the Delhi Ridge (Fig. 2). In contrast, no prominent subsidence zone is observed on the eastern side (between the ridge and Yamuna river), suggesting possible compartmentalization of the underlying aquifer system by Delhi Ridge. As the distribution of subsidence zones is a good indicator of the presence of confined aquifers (Schmidt and Bürgmann, 2003) and the presence of compressible deposits (Amelung et al., 1999), it can be inferred that confined aquifers are more frequent on the western side of the ridge than the eastern side. This inference is also supported by the depth-to-bedrock estimates, which is significantly greater (80–170 m) on the western side of the ridge (CGWB, 2016b) than the eastern side (9.2–80 m). Further, the aquifers on the eastern side of the ridge are sand-dominated, while clay, silt, and “kankar” dominate the aquifers on the western side (CGWB, 2016b). Thus, it is evident that the aquifers located on the eastern and western side of the ridge are different in terms of alluvium thickness, the proportion of fine-grained material, and govern the spatial distribution of subsidence zones. The Delhi Ridge, comprised of hard and resistant folded quartzite, acts as a

groundwater divide. Rainfall on the eastern side is channelized towards the Yamuna river following the regional slope while it enters the natural depressions on the western side. Since groundwater also follows the regional slope, the direction of groundwater flow is opposite on both sides of the ridge (Kumar et al., 2011). Thus the Delhi Ridge effectuates compartmentalization of aquifers on either side.

### 5.4. Lack of seasonal effect

InSAR-derived time series of vertical displacement has been successfully utilized to characterize the seasonal deformation of aquifer systems due to annual recharge and pumping (Smith and Li, 2021; Riel et al., 2018; Bell et al., 2008; Lanari et al., 2004; Hoffmann et al., 2001). For the NCR, the InSAR-derived subsidence do not show any prominent seasonal signals. This indicates that there may be no significant lateral variations in pore pressure of the aquifer system at seasonal time scales, similar to central Mexico (Chaussard et al., 2021; Chaussard et al., 2013; Osmanoğlu et al., 2011). The most likely reason behind the lack of significant seasonal signal is the relentless (non-periodic) groundwater pumping to meet the urban and industrial needs of the region. Alternatively, no pumping is taking place in the regions where aquifers are expected to behave elastically. In the case of non-periodic/continuous pumping, even groundwater inflow from the surrounding aquifer or in-situ recharge may not lead to a significant seasonal rebound of the aquifer as extraction exceeds recharge in such scenarios. The subsidence zones (Gurgaon and Faridabad area) are undergoing inelastic deformation. It is more likely that long-term linear signals will dominate the seasonal signals (Smith and Knight, 2019; Sned, 2001) in these regions. Further, low magnitude seasonal signal in the order of a few mm, due to in-situ recharge or inflow from the surrounding aquifer(s), cannot be distinguished from residual tropospheric noise (Fattah and Amelung, 2015) since both are temporally collocated. The period of recharge (monsoon period) also happens to be the period with the highest

variability in the water vapor content of the troposphere.

The lack of local seasonal signals, however, does not preclude the presence of regional seasonal vertical displacements which have been recorded in the Indo-Gangetic plain by continuous Global Positioning System stations (cGPS) (Saji et al., 2020). The seasonal amplitude in the data obtained from the cGPS station located in NCR (LIAA), operating from 2019 onwards, is ~ 4 to 5 mm (<http://geodesy.unr.edu/NGLS/stationPages/stations/LIAA.sta>). Large amounts of rainfall during the monsoon period are a major source of hydrological mass change in the Indo-Gangetic plain and are considered the dominant cause of basin-wide seasonal uplift and subsidence (Chanard et al., 2014; Bettinelli et al., 2008). Such regional seasonal displacements are associated with movements of the reference point and can't be detected by InSAR which is a relative measurement technique.

## 6. Conclusions

The present study analyses land subsidence measured over the NCR in India using InSAR time series datasets obtained from ALOS-1 and Sentinel-1 satellites. Two notable subsidence zones located in the vicinity of Dwarka and Gurgaon are detected during 2007–10, while an additional subsidence zone located near Faridabad is detected during Nov. 2014–19. The spatiotemporal analysis reveal stabilization of subsidence zone near Dwarka post-Sept. 2016, while the subsidence zones near Gurgaon increased significantly in spatial extent as well as in the rate of subsidence as compared to 2007–10. Results reveal that the stabilization of subsidence near Dwarka is attributed to the reduction in groundwater extraction post-Nov. 2014 and changes in the deformation phase of the aquifer from inelastic to elastic. On the contrary, the subsidence zones near Gurgaon and Faridabad continue to grow with no signs of stabilization. The continuing inelastic deformation noted here is causing permanent loss of storage and is detrimental to the groundwater potential of the area.

The present study demonstrates the use of InSAR-based time series of vertical displacement to map the subsidence-affected regions and understand the aquifer behavior in the densely populated NCR region. It is important to note that the high spatial and temporal resolution of the surface displacement measurements helped decipher the contrasting deformation behavior of Dwarka and Gurgaon regions located nearby. The results presented here also highlight the potential of InSAR to capture the heterogeneity in land subsidence due to varying groundwater extraction rates. The degree of details achieved here is almost impossible with other satellite or sparse ground-based observational networks monitoring the shallow aquifers. Therefore, the capabilities of InSAR to monitor storage variations of deeper (confined) aquifers can complement the existing network of groundwater monitoring wells to provide an integrated assessment of groundwater resources, especially in the data-scarce regions of the world. It is expected that increasing groundwater demand and lack of natural recharge may increase the areal extent and the magnitude of the documented subsidence zones, and continuous monitoring of its spatiotemporal evolution is essential. Hence, this study will provide information at space–time scales crucial for water managers and urban planners for devising actionable groundwater management plans to minimize the ongoing subsidence and mitigate impending damage to civil infrastructure.

## 7. Credit author statement

HR, THS and FA developed the science questions and designed the study. HR and RA performed the data acquisition and analyses. HR and THS did the interpretation and performed refinement of the results. FA and THS provided critical inputs to place the results in the context of existing knowledge gaps. ASV supervised the study. All the authors provided critical discussion, helped to write and revise the manuscript and approved its submission.

## Declaration of Competing Interest

The authors declare that they have no known competing financial interests or personal relationships that could have appeared to influence the work reported in this paper.

## Acknowledgements

Authors would like to thank Shri Dipak Das, Director, SAC and Dr. Raj Kumar, Deputy Director, EPSA/SAC, Dr. A. S. Rajawat, Former GD/GHCAG, Dr. I.M. Bahuguna, GD/GHCAG and Dr. D.R. Rajak, Head/GSD for support and encouragement provided during the course of study, and Bhuvan Varugu for initial data processing. This research was partially funded by Space Application Centre of Indian Space Research Organisation, Government of India, under the Disaster Management Support Programme (R&D) with project number SAC/EPSA/GSD/DMSP/WP/06/2016.

Falk Amelung was supported by NASA through the NISAR science team program (NNX16AK52G). For data processing we used the *Stampeude2* system of the Extreme Science and Engineering Discovery Environment (XSEDE) at the *Texas Advanced Computing Center (TACC)* through allocation TG-EAR200012, supported by the National Science Foundation, United States through grant ACI-1548562. We also thank the European Space Agency (ESA) and the Alaska Satellite Facility Distributed Active Archive Center (ASF DAAC) for providing the Sentinel-1 SAR data. Japan Aerospace Exploration Agency (JAXA), Japan is thankfully acknowledged for providing ALOS-1 data under ALOS RA-6 A.O project to T. H. Syed (PI:3034)

## Data availability

Sentinel-1 datasets are publicly available and can be downloaded from <https://ASF.alaska.edu/>. ALOS-1 data was provided by Japan Aerospace Exploration Agency (JAXA), Japan is under ALOS RA-6 A.O project to T. H. Syed (PI: 3034). The groundwater level dataset used in this study can be obtained from India Water Resources Information System (<https://indiawris.gov.in/wris/#>).

## References

- Amelung, F., Galloway, D.L., Bell, J.W., Zebker, H.A., Lacziak, R.J., 1999. Sensing the ups and downs of Las Vegas: InSAR reveals structural control of land subsidence and aquifer-system deformation. *Geology* 27 (6), 483–486.
- Bawden, G.W., Thatcher, W., Stein, R.S., Hudnut, K.W., Peltzer, G., 2001. Tectonic contraction across Los Angeles after removal of groundwater pumping effects. *Nature* 412 (6849), 812–815. <https://doi.org/10.1038/35090558>.
- Bell, J.W., Amelung, F., Ferretti, A., Bianchi, M., Novali, F., 2008. Permanent scatterer InSAR reveals seasonal and long-term aquifer-system response to groundwater pumping and artificial recharge. *Water Resour. Res.* 44 (2) <https://doi.org/10.1029/2007WR006152>.
- Berardino, P., Fornaro, G., Lanari, R., Sansosti, E., 2002. A new algorithm for surface deformation monitoring based on small baseline differential SAR interferograms. *IEEE Trans. Geosci. Remote Sens.* 40 (11), 2375–2383. <https://doi.org/10.1109/TGRS.2002.803792>.
- Bettinelli, P., Avouac, J.P., Flouzat, M., Bollinger, L., Ramillien, G., Rajaure, S., Sapkota, S., 2008. Seasonal variations of seismicity and geodetic strain in the Himalaya induced by surface hydrology. *Earth Planet. Sci. Lett.* 266 (3–4), 332–344. <https://doi.org/10.1016/j.epsl.2007.11.021>.
- Carlson, G., Shirzaei, M., Ojha, C., Werth, S., 2020. Subsidence-Derived Volumetric Strain Models for Mapping Extensional Fissures and Constraining Rock Mechanical Properties in the San Joaquin Valley, California. *J. Geophys. Res. Solid Earth* 125 (9). <https://doi.org/10.1029/2020JB019980>.
- Castellazzi, P., Longuevergne, L., Martel, R., Rivera, A., Brouard, C., Chaussard, E., 2017. Quantitative mapping of groundwater depletion at the water management scale using a combined GRACE/InSAR approach. *Remote Sens. Environ.* 205, 408–418. <https://doi.org/10.1016/j.rse.2017.11.025>.
- Castellazzi, P., Martel, R., Galloway, D.L., Longuevergne, L., Rivera, A., 2016. Assessing groundwater depletion and dynamics using GRACE and InSAR: Potential and limitations. *Groundwater* 54 (6), 768–780. <https://doi.org/10.1111/gwat.12453>.
- CGWB, 2006. Hydrogeological frame work and groundwater management plan of NCT Delhi, Report, Central Ground Water Board, Ministry of Water Resources, Government of India, New Delhi.

- CGWB, 2012. Ground water information booklet of New Delhi district, NCT, Delhi, Central Ground Water Board, Ministry of Water Resources, Government of India, New Delhi.
- CGWB, 2016a. Ground water year book 2015–16 NCT Delhi, Central Ground Water Board, Ministry of Water Resources, Government of India, New Delhi.
- CGWB, 2016b. Aquifer mapping and ground water management plan of NCT Delhi, Central Ground Water Board, Ministry of Water Resources, Government of India, New Delhi.
- Chanard, K., Avouac, J.P., Ramillien, G., Genrich, J., 2014. Modeling deformation induced by seasonal variations of continental water in the Himalaya region: Sensitivity to Earth elastic structure. *J. Geophys. Res.: Solid Earth* 119 (6), 5097–5113. <https://doi.org/10.1002/2013JB010451>.
- Chatterjee, R., Gupta, B.K., Mohiddin, S.K., Singh, P.N., Shekhar, S., Purohit, R., 2009. Dynamic groundwater resources of National Capital Territory, Delhi: assessment, development and management options. *Environ. Earth Sci.* 59 (3), 669–686. <https://doi.org/10.1007/s12665-009-0064-y>.
- Chatterjee, R.S., Fruneau, B., Rudant, J.P., Roy, P.S., Frison, P.L., Lakhera, R.C., Dadhwala, V.K., Saha, R., 2006. Subsidence of Kolkata (Calcutta) City, India during the 1990s as observed from space by differential synthetic aperture radar interferometry (D-InSAR) technique. *Remote Sens. Environ.* 102 (1–2), 176–185. <https://doi.org/10.1016/j.rse.2006.02.006>.
- Chaussard, E., Amelung, F., Abidin, H., Hong, S.H., 2013. Sinking cities in Indonesia: ALOS PALSAR detects rapid subsidence due to groundwater and gas extraction. *Remote Sens. Environ.* 128, 150–161. <https://doi.org/10.1016/j.rse.2012.10.015>.
- Chaussard, E., Bürgmann, R., Shirzaei, M., Fielding, E.J., Baker, B., 2014. Predictability of hydraulic head changes and characterization of aquifer-system and fault properties from InSAR-derived ground deformation. *J. Geophys. Res.: Solid Earth* 119 (8), 6572–6590. <https://doi.org/10.1002/2014JB011266>.
- Chaussard, E., Havazli, E., Fattah, H., Cabral-Cano, E., Solano-Rojas, D., 2021. Over a Century of Sinking in Mexico City: No Hope for Significant Elevation and Storage Capacity Recovery. *J. Geophys. Res. Solid Earth* 126 (4). <https://doi.org/10.1029/2020JB020648>.
- Chaussard, E., Milillo, P., Bürgmann, R., Perissin, D., Fielding, E.J., Baker, B., 2017. Remote sensing of ground deformation for monitoring groundwater management practices: Application to the Santa Clara Valley during the 2012–2015 California drought. *J. Geophys. Res.: Solid Earth* 122 (10), 8566–8582. <https://doi.org/10.1002/2017JB014676>.
- Chen, C.W., Zebker, H.A., 2000. Network approaches to two-dimensional phase unwrapping: intractability and two new algorithms. *J. Opt. Soc. Am. A* 17 (3), 401–414. <https://doi.org/10.1364/JOSAA.17.000401>.
- Chen, J., Knight, R., Zebker, H.A., Schreuder, W.A., 2016. Confined aquifer head measurements and storage properties in the San Luis Valley, Colorado, from spaceborne InSAR observations. *Water Resour. Res.* 52 (5), 3623–3636. <https://doi.org/10.1002/2015WR018466>.
- Cigna, F., Osmanoğlu, B., Cabral-Cano, E., Dixon, T.H., Ávila-Olivera, J.A., Garduño-Monroy, V.H., DeMets, C., Wdowinski, S., 2012. Monitoring land subsidence and its induced geological hazard with Synthetic Aperture Radar Interferometry: A case study in Morelia, Mexico. *Remote Sens. Environ.* 117, 146–161. <https://doi.org/10.1016/j.rse.2011.09.005>.
- Doin, M.P., Guillaso, S., Jolivet, R., Lasserre, C., Lodge, F., Ducret, G., Grandin, R., 2011. September. Presentation of the small baseline NSBAS processing chain on a case example: the Etna deformation monitoring from 2003 to 2010 using Envisat data. In: Proceedings of the Fringe symposium (pp. 3434–3437). Frascati, Italy: ESA SP-697. A.
- Erban, L.E., Gorelick, S.M., Zebker, H.A., 2014. Groundwater extraction, land subsidence, and sea-level rise in the Mekong Delta, Vietnam. *Environ. Res. Lett.* ITALIC 9 (8), 084010. <https://doi.org/10.1088/1748-9326/9/8/084010>.
- Ezquerro, P., Herrera, G., Marchamalo, M., Tomás, R., Béjar-Pizarro, M., Martínez, R., 2014. A quasi-elastic aquifer deformational behavior: Madrid aquifer case study. *J. Hydrol.* 519, 1192–1204. <https://doi.org/10.1016/j.jhydrol.2014.08.040>.
- Farr, T.G., Rosen, P.A., Caro, E., Crippen, R., Duren, R., Hensley, S., Kobrick, M., Paller, M., Rodriguez, E., Roth, L., Seal, D., Shaffer, S., Shimada, J., Umland, J., Werner, M., Oskin, M., Burbank, D., Alsdorf, D., 2007. The shuttle radar topography mission. *Rev. Geophys.* 45 (2) <https://doi.org/10.1029/2005RG000183>.
- Fattah, H., Amelung, F., 2015. InSAR bias and uncertainty due to the systematic and stochastic tropospheric delay. *J. Geophys. Res. Solid Earth* 120 (12), 8758–8773. <https://doi.org/10.1002/2016GL070121>.
- Fattah, H., Amelung, F., 2013. DEM error correction in InSAR time series. *IEEE Trans. Geosci. Remote Sens.* 51 (7), 4249–4259. <https://doi.org/10.1109/TGRS.2012.2227761>.
- Fernandez, J., Prieto, J.F., Escayao, J., Camacho, A.G., Luzón, F., Tiampo, K.F., Palano, M., Abajo, T., Pérez, E., Velasco, J., Herrero, T., Bru, G., Molina, I., López, J., Rodríguez-Velasco, G., Gómez, I., Mallorquí, J.J., 2018. Modeling the two-and three-dimensional displacement field in Lorca, Spain, subsidence and the global implications. *Sci. Rep.* 8 (1) <https://doi.org/10.1038/s41598-018-33128-0>.
- Fielding, E.J., Blom, R.G., Goldstein, R.M., 1998. Rapid subsidence over oil fields measured by SAR interferometry. *Geophys. Res. Lett.* 25 (17), 3215–3218. <https://doi.org/10.1029/98GL52260>.
- Goldstein, R.M., Werner, C.L., 1998. Radar interferogram filtering for geophysical applications. *Geophys. Res. Lett.* 25 (21), 4035–4038. <https://doi.org/10.1029/1998GL900033>.
- González, P.J., Fernández, J., 2011. Drought-driven transient aquifer compaction imaged using multitemporal satellite radar interferometry. *Geology* 39 (6), 551–554. <https://doi.org/10.1130/G31900.1>.
- Herrera-García, G., Ezquerro, P., Tomás, R., Béjar-Pizarro, M., López-Vinielles, J., Rossi, M., Mateos, R.M., Carreón-Freyre, D., Lambert, J., Teatini, P., Cabral-Cano, E., 2021. Mapping the global threat of land subsidence. *Science* 371 (6524), 34–36. <https://doi.org/10.1126/science.abb8549>.
- Hersbach, H., Bell, B., Berrisford, P., Hirahara, S., Horányi, A., Muñoz-Sabater, J., Nicolas, J., Peubey, C., Radu, R., Schepers, D., Simmons, A., Soci, C., Abdalla, S., Abellán, X., Balsamo, G., Bechtold, P., Biavati, G., Bidlot, J., Bonavita, M., Chiara, G., Dahlgren, P., Dee, D., Diamantakis, M., Dragani, R., Flemming, J., Forbes, R., Fuente, M., Geer, A., Haimberger, L., Healy, S., Hogan, R.J., Holm, E., Janisková, M., Keeley, S., Laloyaux, P., Lopez, P., Lupu, C., Radnoti, G., Rosnay, P., Rozum, I., Vamborg, F., Villaume, S., Thépaut, J.-N., 2020. The ERA5 global reanalysis. *Q. J. R. Meteorol. Soc.* 146 (730), 1999–2049. <https://doi.org/10.1002/qj.3803>.
- Higgins, S.A., Overeem, I., Steckler, M.S., Syvitski, J.P., Seeber, L., Akhter, S.H., 2014. InSAR measurements of compaction and subsidence in the Ganges-Brahmaputra Delta, Bangladesh. *J. Geophys. Res. Earth Surf.* 119 (8), 1768–1781. <https://doi.org/10.1002/2014JF003117>.
- Hoffmann, J., Galloway, D.L., Zebker, H.A., 2003. Inverse modeling of interbed storage parameters using land subsidence observations, Antelope Valley, California. *Water Resour. Res.* 39 (2), 1031. <https://doi.org/10.1029/2001WR001252>.
- Hoffmann, J., Zebker, H.A., Galloway, D.L., Amelung, F., 2001. Seasonal subsidence and rebound in Las Vegas Valley, Nevada, observed by synthetic aperture radar interferometry. *Water Resour. Res.* 37 (6), 1551–1566. <https://doi.org/10.1029/2000WR900404>.
- Hu, X., Lu, Z., Wang, T., 2018. Characterization of hydrogeological properties in salt lake valley, Utah, using InSAR. *J. Geophys. Res. Earth Surf.* 123 (6), 1257–1271. <https://doi.org/10.1029/2017JF004497>.
- Kaul, B.L., Pandit, M.K., 2004. Morphotectonic evaluation of the Delhi region in northern India, and its significance in environmental management. *Environ. Geol.* 46 (8), 1118–1122. <https://doi.org/10.1007/s00254-004-1111-3>.
- Kumar, M., Rao, M.S., Kumar, B., Ramanathan, A., 2011. Identification of aquifer-recharge zones and sources in an urban development area (Delhi, India), by correlating isotopic tracers with hydrological features/identification des aires de recharge d'un aquifère et origine de l'eau en zone de développement urbain (Delhi, Inde), par corrélation entre traçages isotopiques et caractéristiques hydrogéologiques/identificación de zonas de recarga de acuíferos y fuentes en un área con desarrollo urbano (Delhi, India), correlacionando trazadores isotópicos con características hidrológicas/利用同位素示踪剂和水文特征的相关性识别城市发展区(印度德里)含水层的补给区和补给源/Identificação de zonas de recarga de aquíferos e de origens numa área de desenvolvimento urbano (Delhi, Índia), através da correlação de traçadores isotópicos com características hidrológicas. *Hydrogeol. J.* 19 (2), 463–474. <https://doi.org/10.1007/s10040-010-0692-z>.
- Lanari, R., Lundgren, P., Manzo, M., Casu, F., 2004. Satellite radar interferometry time series analysis of surface deformation for Los Angeles, California. *Geophys. Res. Lett.* 31 (23) <https://doi.org/10.1029/2004GL021294>.
- Lundgren, P., Usai, S., Sansosti, E., Lanari, R., Tesauro, M., Fornaro, G., Berardino, P., 2001. Modeling surface deformation observed with synthetic aperture radar interferometry at Campi Flegrei caldera. *J. Geophys. Res. Solid Earth* 106 (B9), 19355–19366.
- Lu, Z., Danskin, W.R., 2001. InSAR analysis of natural recharge to define structure of a ground-water basin, San Bernardino, California. *Geophys. Res. Lett.* 28 (13), 2661–2664. <https://doi.org/10.1029/2000GL012753>.
- Menke, W., 2018. *Geophysical data analysis: Discrete inverse theory*. Academic Press.
- Miller, M.M., Shirzaei, M., 2015. Spatiotemporal characterization of land subsidence and uplift in Phoenix using InSAR time series and wavelet transforms. *J. Geophys. Res. Solid Earth* 120 (8), 5822–5842. <https://doi.org/10.1002/2015JB012017>.
- Miller, M.M., Shirzaei, M., Argus, D., 2017. Aquifer mechanical properties and decelerated compaction in Tucson, Arizona. *J. Geophys. Res. Solid Earth* 122 (10), 8402–8416. <https://doi.org/10.1002/2017JB014531>.
- Murray, K.D., Lohman, R.B., 2018. Short-lived pause in Central California subsidence after heavy winter precipitation of 2017. *Sci. Adv.* 4 (8), p.eaar8144. <https://doi.org/10.1126/sciadv.aar8144>.
- Ojha, C., Werth, S., Shirzaei, M., 2020. Recovery of aquifer-systems in Southwest US following 2012–2015 drought: Evidence from InSAR, GRACE and groundwater level data. *J. Hydrol.* 587, 124943. <https://doi.org/10.1016/j.jhydrol.2020.124943>.
- Osmanoğlu, B., Dixon, T.H., Wdowinski, S., Cabral-Cano, E., Jiang, Y., 2011. Mexico City subsidence observed with persistent scatterer InSAR. *Int. J. Appl. Earth Obs. Geoinf.* 13 (1), 1–12. <https://doi.org/10.1016/j.jag.2010.05.009>.
- Poland, J.F., Ireland, R.L., 1988. Land subsidence in the Santa Clara Valley, California, as of 1982 (Vol. 497). Department of the Interior, US Geological Survey.
- Reeves, J.A., Knight, R., Zebker, H.A., Kitadis, P.K., Schreider, W.A., 2014. Estimating temporal changes in hydraulic head using InSAR data in the San Luis Valley, Colorado. *Water Resour. Res.* 50 (5), 4459–4473. <https://doi.org/10.1002/2013WR014938>.
- Riel, B., Simons, M., Ponti, D., Agram, P., Jolivet, R., 2018. Quantifying ground deformation in the Los Angeles and Santa Ana Coastal Basins due to groundwater withdrawal. *Water Resour. Res.* 54 (5), 3557–3582. <https://doi.org/10.1029/2017WR021978>.
- Riyas, M.J., Syed, T.H., Kumar, H., Kuenzer, C., 2021. Detecting and Analyzing the Evolution of Subsidence Due to Coal Fires in Jharia Coalfield, India Using Sentinel-1 SAR Data. *Remote Sens.* 2021 (13), 1521. <https://doi.org/10.3390/rs13081521>.
- Rodell, M., Velicogna, I., Famiglietti, J.S., 2009. Satellite-based estimates of groundwater depletion in India. *Nature* 460 (7258), 999–1002. <https://doi.org/10.1038/nature08238>.
- Rosen, P.A., Gurrola, E., Sacco, G.F., Zebker, H., 2012, April. The InSAR scientific computing environment. In: EUSAR 2012; 9th European Conference on Synthetic Aperture Radar (pp. 730–733). VDE.

- Saji, A.P., Sunil, P.S., Sreejith, K.M., Gautam, P.K., Kumar, K.V., Ponraj, M., Amirtharaj, S., Shaju, R.M., Begum, S.K., Reddy, C.D., Ramesh, D.S., 2020. Surface deformation and influence of hydrological mass over Himalaya and North India revealed from a decade of continuous GPS and GRACE observations. e2018JF004943. *J. Geophys. Res.: Earth Surf.* 125 (1). <https://doi.org/10.1029/2018JF004943>.
- Schmidt, D.A., Bürgmann, R., 2003. Time-dependent land uplift and subsidence in the Santa Clara valley, California, from a large interferometric synthetic aperture radar data set. *J. Geophys. Res. Solid Earth* 108 (B9). <https://doi.org/10.1029/2002JB002267>.
- Shekhar, S., Prasad, R.K., 2009. The groundwater in the Yamuna flood plain of Delhi (India) and the management optionsL'eau souterraine dans le lit majeur de la Yamuna à Delhi (Inde) et les options de gestionEl agua subterránea en la llanura aluvial Yamuna de Delhi (India) y las opciones de gestión印度德里雅沐拿河冲积平原地下水及其管理途径A água subterrânea na planície de inundação de Yamuna em Deli (India) e as opções de gestão. *Hydrogeology* 17 (7), 1557–1560. <https://doi.org/10.1007/s10040-008-0430-y>.
- Shirzaei, M., Bürgmann, R., 2018. Global climate change and local land subsidence exacerbate inundation risk to the San Francisco Bay Area. *Sci. Adv.* 4 (3), p. eaap9234. <https://doi.org/10.1126/sciadv.aap9234>.
- Shirzaei, M., Bürgmann, R., Fielding, E.J., 2017. Applicability of Sentinel-1 terrain observation by progressive scans multitemporal interferometry for monitoring slow ground motions in the San Francisco Bay Area. *Geophys. Res. Lett.* 44 (6), 2733–2742. <https://doi.org/10.1002/2017GL072663>.
- Shirzaei, M., Ojha, C., Werth, S., Carlson, G., Vivoni, E.R., 2019. Comment on "Short-lived pause in Central California subsidence after heavy winter precipitation of 2017" by KD Murray and RB Lohman. *Sci. Adv.* 5 (6), p.eaa8038. <https://doi.org/10.1126/sciadv.aav8038>.
- Simons, M., Rosen, P., 2007. Interferometric synthetic aperture radar geodesy. In: *Treatise on Geophysics*, vol. 3, edited by T. Herring, chap. 12, 391–446, Elsevier, New York.
- Smith, R.G., Knight, R., Chen, J., Reeves, J.A., Zebker, H.A., Farr, T., Liu, Z., 2017. Estimating the permanent loss of groundwater storage in the southern San Joaquin Valley, California. *Water Resour. Res.* 53 (3), 2133–2148. <https://doi.org/10.1002/2016WR019861>.
- Smith, R., Knight, R., 2019. Modeling land subsidence using InSAR and airborne electromagnetic data. *Water Resour. Res.* 55 (4), 2801–2819. <https://doi.org/10.1029/2018WR024185>.
- Smith, R., Li, J., 2021. Modeling elastic and inelastic pumping-induced deformation with incomplete water level records in Parowan Valley, Utah. *J. Hydrol.* 601, 126654. <https://doi.org/10.1016/j.jhydrol.2021.126654>.
- Sneed, M., 2001. Hydraulic and mechanical properties affecting ground-water flow and aquifer-system compaction, San Joaquin Valley, California, U.S. Geol. Surv. Open File Rep. 01-35, 5–17.
- Soni, A., Syed, T.H., 2015. Diagnosing land water storage variations in major Indian river basins using GRACE observations. *Glob. Planet. Change* 133, 263–271. <https://doi.org/10.1016/j.gloplacha.2015.09.007>.
- Suganthi, S., Elango, L., 2020. Estimation of groundwater abstraction induced land subsidence by SBAS technique. *J. Earth Syst. Sci.* 129 (1), 1–13. <https://doi.org/10.1007/s12040-019-1298-z>.
- Teatini, P., Tosi, L., Strozzi, T., 2011. Quantitative evidence that compaction of Holocene sediments drives the present land subsidence of the Po Delta, Italy. *J. Geophys. Res. Solid Earth* 116 (B8). <https://doi.org/10.1029/2010JB008122>.
- Terzaghi, K., 1925. *Principles of soil mechanics: IV, Settlement and consolidation of clay*, McGraw-Hill, New York, v. 95.
- Tiwari, V.M., Wahr, J., Swenson, S., 2009. Dwindling groundwater resources in northern India, from satellite gravity observations. *Geophys. Res. Lett.* 36 (18). <https://doi.org/10.1029/2009GL039401>.
- UNESCO, 2017. International Hydrological Program VIII (2014–2020). Available at: <http://en.unesco.org/themes/water-security/hydrology>.
- Usai, S., 2003. A least squares database approach for SAR interferometric data. *IEEE Trans. Geosci. Remote Sens.* 41 (4), 753–760. <https://doi.org/10.1109/TGRS.2003.810675>.
- Wilson, A.M., Gorelick, S., 1996. The effects of pulsed pumping on land subsidence in the Santa Clara Valley, California. *J. Hydrol.* 174 (3–4), 375–396. [https://doi.org/10.1016/0022-1694\(95\)02722-X](https://doi.org/10.1016/0022-1694(95)02722-X).
- Yunjun, Z., Fattah, H., Amelung, F., 2019. Small baseline InSAR time series analysis: Unwrapping error correction and noise reduction. *Comput. Geosci.* 133, 104331. <https://doi.org/10.1016/j.cageo.2019.104331>.